

## Surfactant–Polymer Nanoparticles Enhance the Effectiveness of Anticancer Photodynamic Therapy

Ayman Khdair,<sup>†,‡</sup> Brigitte Gerard,<sup>§</sup> Hitesh Handa,<sup>||</sup> Guangzhao Mao,<sup>||</sup>  
Malathy P. V. Shekhar,<sup>§,⊥</sup> and Jayanth Panyam<sup>\*,‡</sup>

Department of Pharmaceutical Sciences, Eugene Applebaum College of Pharmacy and Health Sciences, Wayne State University, Detroit, Michigan 48201, Department of Pharmaceutics, College of Pharmacy, University of Minnesota, Minneapolis, Minnesota 55455, Breast Cancer Program, Karmanos Cancer Institute, 110 East Warren Avenue, Detroit, Michigan 48201, Department of Chemical Engineering and Materials Science, College of Engineering, Wayne State University, Detroit, Michigan 48202, and Department of Pathology, Wayne State University School of Medicine, Detroit, Michigan 48201

Received February 22, 2008; Revised Manuscript Received May 13, 2008; Accepted May 27, 2008

**Abstract:** Photodynamic therapy (PDT) is a promising treatment modality for cancer. PDT is based on the concept that photosensitizers, when exposed to light of specific wavelength, generate cytotoxic reactive oxygen species (ROS) capable of killing tumor cells. The effectiveness of PDT has been limited in part by the lack of photosensitizers that accumulate sufficiently in tumor cells and poor yield of ROS from existing photosensitizers. In this report, we investigated whether aerosol OT-alginate nanoparticles can be used as a carrier to enhance the therapeutic efficacy of a model photosensitizer, methylene blue. Methylene blue loaded nanoparticles were evaluated for PDT effectiveness in two cancer cell lines, MCF-7 and 4T1. Encapsulation of methylene blue in nanoparticles significantly enhanced intracellular ROS production, and the overall cytotoxicity following PDT. It also resulted in higher incidence of necrosis. Greater effectiveness of nanoparticles could be correlated with higher yield of ROS with nanoparticle-encapsulated methylene blue. Further, treatment of tumor cells with nanoparticle-encapsulated methylene blue resulted in significant nuclear localization of methylene blue while free drug treatment resulted in its accumulation mainly in the endolysosomal vesicles. In conclusion, encapsulation of methylene blue in aerosol OT-alginate nanoparticles enhanced its anticancer photodynamic efficacy *in vitro*. Increased ROS production and favorable alteration in the subcellular distribution contribute to the enhanced PDT efficacy of nanoparticle-encapsulated photosensitizer.

**Keywords:** Reactive oxygen species; photosensitizer; cancer therapy; cellular delivery; cytotoxicity

### Introduction

Photodynamic therapy (PDT), a promising detection and treatment modality for cancer, has been investigated since

\* Author to whom correspondence should be addressed. Mailing address: Department of Pharmaceutics, College of Pharmacy, 308 Harvard St. SE, Minneapolis, MN 55455. Phone: 612-624-0951. Fax: 612-626-2251. E-mail: jpanyam@umn.edu.

<sup>†</sup> Eugene Applebaum College of Pharmacy and Health Sciences, Wayne State University.

<sup>‡</sup> University of Minnesota.

<sup>§</sup> Karmanos Cancer Institute.

<sup>||</sup> College of Engineering, Wayne State University.

the early 20th century.<sup>1,2</sup> PDT is currently used in the clinic as an adjunctive therapy for the treatment of a variety of solid tumors including inoperable esophageal tumors, head and neck cancers, and microinvasive endobronchial non-small cell lung carcinoma.<sup>3</sup> In addition, PDT is being investigated for the treatment of several other cancer types including breast and prostate cancers.<sup>4,5</sup> PDT is based on the concept that certain compounds, called photosensitizers, when exposed to light of specific wavelength, are capable of generating cytotoxic singlet oxygen species (<sup>1</sup>O<sub>2</sub>) and other

<sup>⊥</sup> Wayne State University School of Medicine.

reactive oxygen species (ROS).<sup>6-9</sup> Because it is possible to expose the photosensitizer to light and activate it specifically in the target tumor tissue, PDT can be used to kill tumor cells selectively.

While there is an increasing appreciation of the usefulness of PDT for tumor therapy, clinical use of PDT has been limited. An ideal photosensitizer should satisfy several criteria: chemical purity, tumor selectivity, minimal dark toxicity, rapid systemic clearance, high photochemical reactivity and activation at longer wavelengths.<sup>10</sup> Currently available photosensitizers only partially fulfill these criteria. Many new PDT agents have been investigated including chlorins and phthalocyanines, with favorable PDT properties.<sup>11</sup> Methylene blue, a water-soluble phenothiazine derivative, has been used for a variety of clinical applications, including PDT.<sup>10,12</sup> Methylene blue is approved by the FDA for use in methemoglobinemia. The high quantum yield of

<sup>1</sup>O<sub>2</sub> generation ( $\Phi_{\Delta} \sim 0.5$ ),<sup>13</sup> coupled with relatively low dark toxicity,<sup>14</sup> makes methylene blue an attractive candidate for PDT. However, clinical use of methylene blue for PDT has been limited because of lack of significant therapeutic efficacy following systemic administration. Methylene blue accumulates extensively in erythrocytes<sup>15</sup> and endothelial cells,<sup>16,17</sup> where it is reduced to leucomethylene blue, resulting in the loss of photodynamic activity.<sup>12</sup>

A potential approach to enhance the efficacy of photosensitizers like methylene blue is to encapsulate them in a drug carrier such as nanoparticles. Carrier-mediated delivery allows increased accumulation of the photosensitizer in the tumor tissue through the “enhanced permeation and retention” effect.<sup>18</sup> The photosensitizer does not have to dissociate from the carrier for activation to occur,<sup>19</sup> and additional efficacy can be achieved because of the potential for increased cell penetration and retention observed with nanoparticles.<sup>20</sup> Further, incorporation of methylene blue in nanoparticles is expected to reduce its degradation in the biological environment<sup>21</sup> and enable greater availability in the tumor tissue.

We have recently reported the fabrication of a novel surfactant–polymer nanoparticle system for efficient encapsulation and sustained release of charged, polar molecules like methylene blue.<sup>22</sup> These nanoparticles are formulated using dioctyl sodium sulfosuccinate (aerosol OT; AOT) and sodium alginate. AOT is an anionic surfactant that is

- (1) Ackroyd, R.; Kelty, C.; Brown, N.; Reed, M. The history of photodetection and photodynamic therapy. *Photochem. Photobiol.* **2001**, *74*, 656–669.
- (2) Wiedmann, M. W.; Caca, K. General principles of photodynamic therapy (PDT) and gastrointestinal applications. *Curr. Pharm. Biotechnol.* **2004**, *5*, 397–408.
- (3) Brown, S. B.; Brown, E. A.; Walker, I. The present and future role of photodynamic therapy in cancer treatment. *Lancet Oncol.* **2004**, *5*, 497–508.
- (4) Dolmans, D. E.; Fukumura, D.; Jain, R. K. Photodynamic therapy for cancer. *Nat. Rev. Cancer* **2003**, *3*, 380–387.
- (5) Allison, R.; Mang, T.; Hewson, G.; Snider, W.; Dougherty, D. Photodynamic therapy for chest wall progression from breast carcinoma is an underutilized treatment modality. *Cancer* **2001**, *91*, 1–8.
- (6) An, H.; Xie, J.; Zhao, J.; Li, Z. Photogeneration of free radicals (\*OH and HB\*-) and singlet oxygen (1O<sub>2</sub>) by hypocrellin B in TX-100 micelles microsurrroundings. *Free Radical Res.* **2003**, *37*, 1107–1112.
- (7) Chekulayeva, L. V.; Shevchuk, I. N.; Chekulayev, V. A.; Ilmarinen, K. Hydrogen peroxide, superoxide, and hydroxyl radicals are involved in the phototoxic action of hematoporphyrin derivative against tumor cells. *J. Environ. Pathol. Toxicol. Oncol.* **2006**, *25*, 51–77.
- (8) Diamond, I.; Granelli, S. G.; McDonagh, A. F.; Nielsen, S.; Wilson, C. B.; Jaenicke, R. Photodynamic therapy of malignant tumours. *Lancet* **1972**, *2*, 1175–1177.
- (9) You, Y.; Gibson, S. L.; Hilf, R.; Davies, S. R.; Oseroff, A. R.; Roy, I.; Ohulchanskyy, T. Y.; Bergey, E. J.; Detty, M. R. Water soluble, core-modified porphyrins. 3. Synthesis, photophysical properties, and in vitro studies of photosensitization, uptake, and localization with carboxylic acid-substituted derivatives. *J. Med. Chem.* **2003**, *46*, 3734–3747.
- (10) Sharman, W. M.; Allen, C. M.; van Lier, J. E. Photodynamic therapeutics: basic principles and clinical applications. *Drug Discovery Today* **1999**, *4*, 507–517.
- (11) Bonnett, R. Photosensitizers of the porphyrin and phthalocyanine series for photodynamic therapy. *Chem. Soc. Rev.* **1995**, *24*, 19–33.
- (12) Gabrielli, D.; Belisle, E.; Severino, D.; Kowaltowski, A. J.; Baptista, M. S. Binding, aggregation and photochemical properties of methylene blue in mitochondrial suspensions. *Photochem. Photobiol.* **2004**, *79*, 227–232.
- (13) Redmond, R. W.; Gamlin, J. N. A Compilation of Singlet Oxygen Yields from Biologically Relevant Molecules. *Photochem. Photobiol.* **1999**, *70*, 391–475.
- (14) DeRosa, M. C.; Crutchley, R. J. Photosensitized singlet oxygen and its applications. *Coord. Chem. Rev.* **2002**, *233–234*, 351–371.
- (15) Sass, M. D.; Caruso, C. J.; Axelrod, D. R. Accumulation of methylene blue by metabolizing erythrocytes. *J. Lab. Clin. Med.* **1967**, *69*, 447–455.
- (16) Bongard, R. D.; Merker, M. P.; Shundo, R.; Okamoto, Y.; Roerig, D. L.; Linehan, J. H.; Dawson, C. A. Reduction of thiazine dyes by bovine pulmonary arterial endothelial cells in culture. *Am. J. Physiol.* **1995**, *269*, L78–L84.
- (17) Olson, L. E.; Merker, M. P.; Patel, M. K.; Bongard, R. D.; Daum, J. M.; Johns, R. A.; Dawson, C. A. Cyanide increases reduction but decreases sequestration of methylene blue by endothelial cells. *Ann. Biomed. Eng.* **2000**, *28*, 85–93.
- (18) Iyer, A. K.; Khaled, G.; Fang, J.; Maeda, H. Exploiting the enhanced permeability and retention effect for tumor targeting. *Drug Discovery Today* **2006**, *11*, 812–818.
- (19) Tang, W.; Xu, H.; Kopelman, R.; Philbert, M. A. Photodynamic characterization and in vitro application of methylene blue-containing nanoparticle platforms. *Photochem. Photobiol.* **2005**, *81*, 242–249.
- (20) Panyam, J.; Labhasetwar, V. Dynamics of endocytosis and exocytosis of poly(D,L-lactide-co-glycolide) nanoparticles in vascular smooth muscle cells. *Pharm. Res.* **2003**, *20*, 212–220.
- (21) Wagner, S. J.; Skripchenko, A.; Robinette, D.; Foley, J. W.; Cincotta, L. Factors affecting virus photoinactivation by a series of phenothiazine dyes. *Photochem. Photobiol.* **1998**, *67*, 343–349.
- (22) Chavanpatil, M. D.; Khdair, A.; Patil, Y.; Handa, H.; Mao, G.; Panyam, J. Polymer-surfactant nanoparticles for sustained release of water-soluble drugs. *J. Pharm. Sci.* **2007**, *96*, 3379–3389.

approved as oral, topical and intramuscular excipient. Sodium alginate is a naturally occurring polysaccharide polymer that has been extensively used in drug delivery.<sup>23,24</sup> Our previous studies have shown that AOT–alginate nanoparticles can sustain the release of water-soluble molecules over a period of weeks.<sup>22,25</sup> In addition, AOT–alginate nanoparticles can significantly improve the cellular accumulation and retention of water-soluble molecules in tumor cells, resulting in enhanced therapeutic efficacy.<sup>25</sup> Based on those favorable properties, we rationalized that AOT–alginate nanoparticles would significantly improve the PDT efficacy of methylene blue. Interestingly, we observed that encapsulation of methylene blue in AOT–alginate nanoparticles not only improves its cellular delivery but also increases its ROS yield, resulting in a significant enhancement in PDT efficacy.

## Materials and Methods

**Materials.** Methylene blue, sodium alginate, polyvinyl alcohol, and calcein AM were purchased from Sigma-Aldrich

- (23) Iskakov, R. M.; Kikuchi, A.; Okano, T. Time-programmed pulsatile release of dextran from calcium-alginate gel beads coated with carboxy-n-propylacrylamide copolymers. *J. Controlled Release* **2002**, *80*, 57–68.
- (24) Shimizu, T.; Yamato, M.; Kikuchi, A.; Okano, T. Cell sheet engineering for myocardial tissue reconstruction. *Biomaterials* **2003**, *24*, 2309–2316.
- (25) Chavanpatil, M. D.; Khadair, A.; Panyam, J. Surfactant-polymer nanoparticles: a novel platform for sustained and enhanced cellular delivery of water-soluble molecules. *Pharm. Res.* **2007**, *24*, 803–810.
- (26) Yamamoto, J.; Yamamoto, S.; Hirano, T.; Li, S.; Koide, M.; Kohno, E.; Okada, M.; Inenaga, C.; Tokuyama, T.; Yokota, N.; Terakawa, S.; Namba, H. Monitoring of singlet oxygen is useful for predicting the photodynamic effects in the treatment for experimental glioma. *Clin. Cancer Res.* **2006**, *12*, 7132–7139.
- (27) Niedre, M. J.; Yu, C. S.; Patterson, M. S.; Wilson, B. C. Singlet oxygen luminescence as an in vivo photodynamic therapy dose metric: validation in normal mouse skin with topical aminolevulinic acid. *Br. J. Cancer* **2005**, *92*, 298–304.
- (28) Folkes, L. K.; Wardman, P. Enhancing the efficacy of photodynamic cancer therapy by radicals from plant auxin (indole-3-acetic acid). *Cancer Res.* **2003**, *63*, 776–779.
- (29) Williams, J. L.; Stamp, J.; Devonshire, R.; Fowler, G. J. Methylene blue and the photodynamic therapy of superficial bladder cancer. *J. Photochem. Photobiol. B* **1989**, *4*, 229–232.
- (30) Mellish, K. J.; Cox, R. D.; Vernon, D. I.; Griffiths, J.; Brown, S. B. In vitro photodynamic activity of a series of methylene blue analogues. *Photochem. Photobiol.* **2002**, *75*, 392–397.
- (31) Afonso, S. G.; Enriquez de Salamanca, R.; Battlle, A. M. The photodynamic and non-photodynamic actions of porphyrins. *Braz. J. Med. Biol. Res.* **1999**, *32*, 255–266.
- (32) Kirszberg, C.; Rumjanek, V. M.; Capella, M. A. M. Methylene blue is more toxic to erythrocytic cells than to normal peripheral blood mononuclear cells: a possible use in chemotherapy. *Cancer Chemother. Pharmacol.* **2005**, *56*, 659–665.
- (33) Kontos, H. A.; Wei, E. P. Hydroxyl radical-dependent inactivation of guanylate cyclase in cerebral arterioles by methylene blue and by LY83583. *Stroke* **1993**, *24*, 427–434.
- (34) Weber, G.; Nakamura, H.; Natsumeda, Y.; Szekeres, T.; Nagai, M. Regulation of GTP biosynthesis. *Adv. Enzyme Regul.* **1992**, *32*, 57–69.

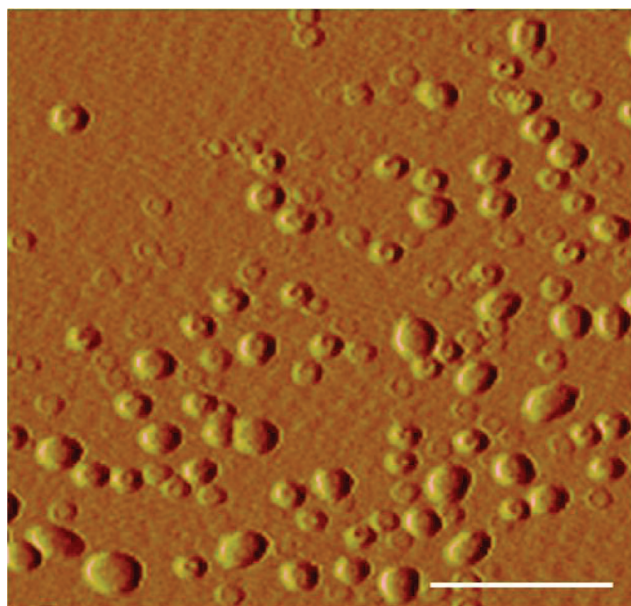


**Figure 1.** AFM image of methylene blue-loaded nanoparticles in the tapping mode in air. The image is an amplitude image of a representative sample spot. Length of the bar is 500 nm.

(St. Louis, MO). AOT was purchased from Fisher Scientific (Chicago, IL). 3'-(*p*-Aminophenyl)fluorescein (APF), 5-(and-6)-chloromethyl-2',7'-dichlorodihydrofluorescein diacetate, acetyl ester (CM-H<sub>2</sub>DCFDA), LysoTracker Green, DAPI (4',6-diamidino-2-phenylindole), and Singlet Oxygen Sensor Green Reagent (SOSGR) were purchased from Invitrogen (Carlsbad, CA). CellTiter 96 AQueous was purchased from Promega (Madison, WI). Propidium iodide was purchased from Roche Diagnostics Corporation (Indianapolis, IN).

**Methods. Nanoparticle Formulation.** Nanoparticles were formulated by a multiple-emulsion cross-linking process developed in our laboratory.<sup>22</sup> Briefly, an aqueous solution (1 mL) of methylene blue (5 mg) and sodium alginate (10 mg) was emulsified into AOT solution in methylene chloride (2.5% w/v; 2 mL) by sonication (Sonicator 3000, Misonix, Farmingdale, NY) for 1 min over an ice bath. The water-in-oil emulsion was further emulsified into aqueous solution of polyvinyl alcohol (PVA) (2% w/v; 15 mL) by sonication for 1 min over an ice bath to form a water-in-oil-in-water emulsion. Five milliliters of aqueous calcium chloride solution (60% w/v) was gradually added to the final emulsion with stirring. Methylene chloride was evaporated by stirring at ambient conditions overnight and then under vacuum for 1 h. The nanoparticle suspension was subjected to ultracentrifugation (145000g for 30 min, Beckman, Palo Alto, CA) three times and reconstituted after each time with deionized water to remove excess methylene blue and polyvinyl alcohol. The pellet from the last ultracentrifugation step was reconstituted in deionized water, and nanoparticles were separated from aggregates and large microparticles by centrifugation (1000 rpm for 3 min, Eppendorf 5810 R, Eppendorf, Westbury, NY). Dry nanoparticle formulation was obtained by lyophilization (FreeZone 4.5, Labconco,

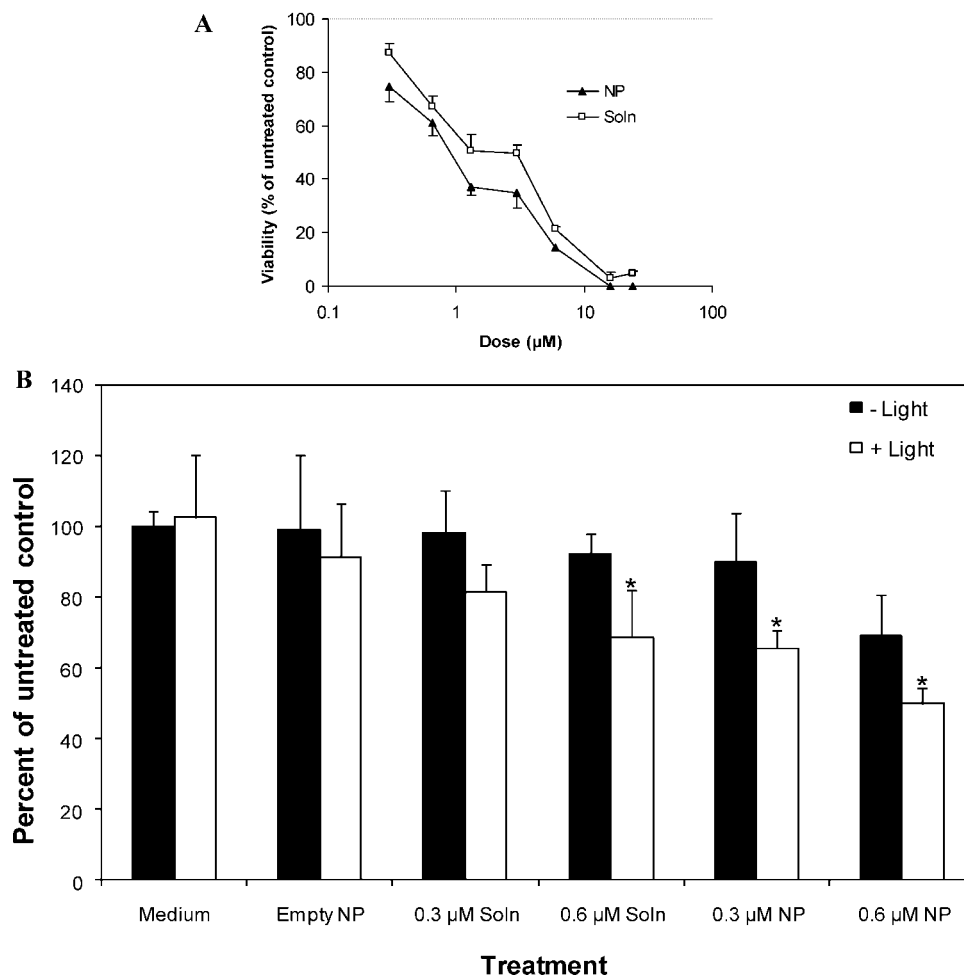


**Figure 2.** (A) Dose–response curve demonstrating enhanced cytotoxicity following PDT with nanoparticle-encapsulated methylene blue. MCF-7 cells were treated for 24 h with methylene blue in solution (Soln) or equivalent doses loaded in nanoparticles (NP). Cells treated with growth medium or empty nanoparticles were used as respective controls. Viability of treated cells is represented as a percent of the respective control. Data as mean ± SEM (*n* = 7 wells). (B) MCF-7 cells were treated for 24 h with growth medium (Medium), blank nanoparticles (Empty NP), methylene blue in solution (Soln; 0.3 or 0.6 µM) or equivalent doses loaded in nanoparticles (NP). Some of the cells were then exposed to light (1200 mJ/cm<sup>2</sup>). Cell viability was quantified using MTS assay. Data as mean ± SD (*n* = 8 wells). \**P* < 0.05.

Kansas City, MO) of the supernatant. Nanoparticles were stable to lyophilization and were easily dispersible in aqueous buffers or serum-containing medium following lyophilization.

**Nanoparticle Characterization.** Particle size was determined by dynamic light scattering and atomic force microscopy (AFM) in the tapping mode. For dynamic light scattering studies, a Brookhaven 90Plus (Brookhaven Instruments, Holtsville, NY) instrument was used in the particle size mode. Briefly, 1 mg of nanoparticles was dispersed in 10 mL of deionized water by sonication and was then subjected to particle size determination. Data was analyzed using non-negatively constrained least-squares (NNLS) fit. For AFM studies, silicon tapping tips (TESP, VEECO) were used with a nominal tip radius less than 10 nm. Briefly, a droplet of an aqueous suspension of nanoparticles (100 µg/mL) was spread over a polyethyleneimine-coated glass coverslip and then air-dried. Nanoparticles were then imaged using Nanoscope III (Digital Instruments/VEECO) with an

E scanner (maximum scan area = 14.2 × 14.2 µm<sup>2</sup>). The scan rate was 1 Hz, and the integral and proportional gains were approximately 0.4 and 0.7, respectively. Height images were plane-fit in the fast scan direction with no additional image filtering. Diameters of at least 50 particles were measured in ten random fields to calculate the number-average particle size.

Zeta potential was determined using electrophoretic light scattering. Briefly, 1 mg of nanoparticles was suspended in 1 mL of deionized water by sonication and then subjected to zeta potential analysis using Brookhaven 90Plus in the zeta potential mode.

Methylene blue loading in nanoparticles was determined by extracting 5 mg of nanoparticles in 5 mL of methanol for 1 h in the dark at room temperature. Methylene blue concentration in the methanolic extract was determined using HPLC. A Beckman Coulter HPLC system with System Gold 125 solvent module and 508 autoinjector connected to 168

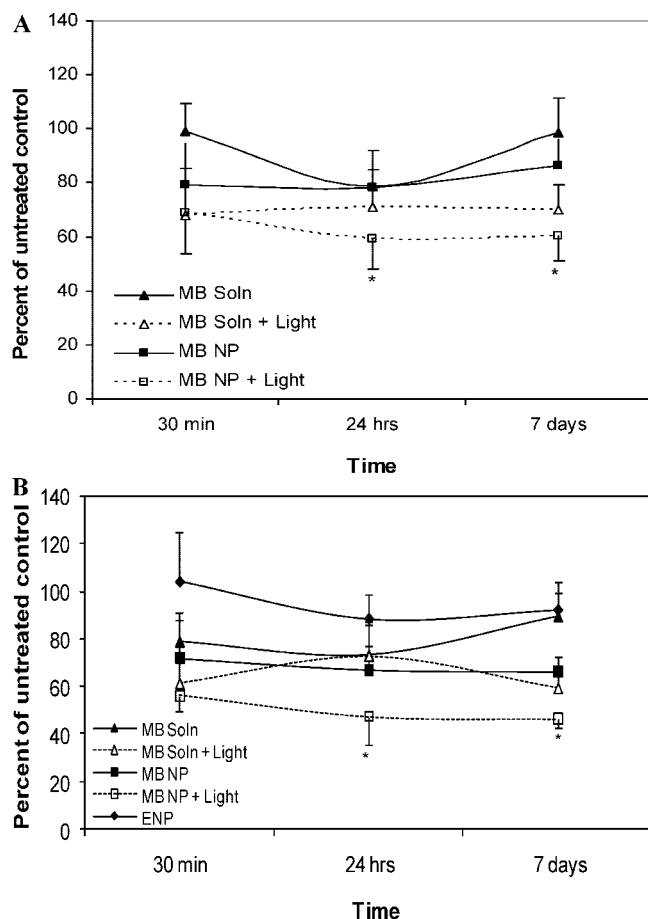


**Figure 3.** Sustained cytotoxicity following PDT with nanoparticle-encapsulated methylene blue. MCF-7 cells were treated for 24 h with (A) 0.3  $\mu\text{M}$  or (B) 0.6  $\mu\text{M}$  methylene blue in nanoparticles (MB NP) or in solution (MB Soln). Cells treated with growth medium and cells treated with blank nanoparticles were used as controls. Some of the cells were then exposed to light (1200  $\text{mJ}/\text{cm}^2$ ). Cell viability was quantified over a period of 7 days using MTS assay. Data as mean  $\pm$  SD ( $n = 8$  wells). \* $P < 0.05$ .

PDA detector was used. A Beckman C-18 (Ultrasphere) column (ODS 4.6  $\times$  250 mm) and UV detection at 598 nm wavelength were used. A mobile phase consisting of acetonitrile and ammonium acetate (10 mM, adjusted to pH 4 with glacial acetic acid) in a 78:22 ratio was used at a flow rate of 1 mL/min. Retention time for methylene blue under these conditions was  $\sim$ 8 min. Drug loading in nanoparticles (w/w) was defined as the amount of methylene blue (mg) in 100 mg of nanoparticles.

**Cytotoxicity Studies.** Human breast cancer cells (MCF-7) and mouse metastatic mammary tumor cells (4T1) were used. Cells were seeded in 96-well plates (5,000 cells/well/0.1 mL) in RPMI 1640 media containing 5% fetal bovine serum. Following attachment, cells were incubated with fresh medium containing different doses of methylene blue in solution or encapsulated in nanoparticles. Untreated cells and cells treated with an equivalent amount of blank nanoparticles were used as controls. Following incubation for 24 h, cells

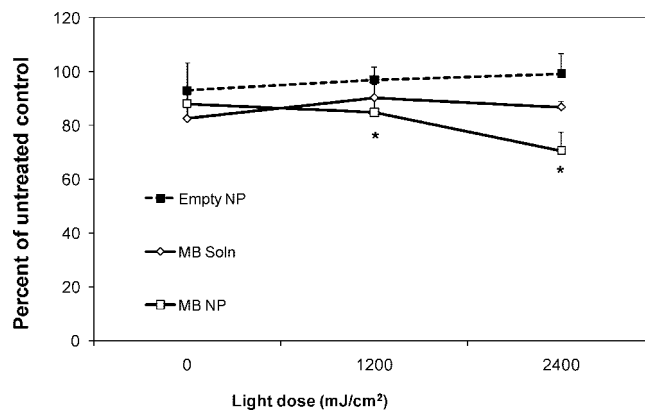


**Figure 4.** Effect of dose of light on methylene blue-mediated PDT. MCF-7 cells were incubated for 24 h with growth medium containing methylene blue in solution (MB Soln) or in nanoparticles (MB NP). Some of the cells were then exposed to 2 different doses of light: 1200 or 2400  $\text{mJ}/\text{cm}^2$ . Some cells were not exposed to light (0  $\text{mJ}/\text{cm}^2$ ). Cells treated with growth medium and cells treated with empty nanoparticles (Empty NP) were used as controls. Cell viability was quantified 24 h following light exposure using MTS assay. Viability data is presented as a percent of medium-treated cells. Data as mean  $\pm$  SD ( $n = 8$  wells). \* $P < 0.05$ .

were washed twice with phosphate buffered saline (PBS) and exposed to different doses of light of 665 nm wavelength (LumaCare LC-122, Newport Beach, CA). Energy of light (fluence) was measured using the light dosimetry equation [fluence ( $\text{J}/\text{cm}^2$ ) = power density ( $\text{W}/\text{cm}^2$ )  $\times$  exposure time (s); 1 W (watt) = 1 J (joule)/s]; power density was fixed at 4  $\text{mW}/\text{cm}^2$ , and exposure time was varied to obtain different light doses. Cells that received similar treatments as above but without the light exposure were used as dark controls. Cell viability was determined at different times following light exposure using CellTiter 96 MTS assay kit.

Induction of necrosis was determined using calcein AM-propidium iodide assay. Calcein AM gets converted to green fluorescent calcein in live cells while necrotic cells and cells in the late stages of apoptosis take up propidium iodide. MCF-7 cells were seeded in 6-well plates (200,000 cells/well/3 mL). Following treatment with 0.3  $\mu\text{M}$  methylene blue in nanoparticles or in solution for 24 h, cells were washed twice with PBS and exposed to a light dose of 1200  $\text{mJ}/\text{cm}^2$ . Cells were then incubated for 24 h at 37  $^\circ\text{C}$ , and then treated with 1  $\mu\text{M}$  calcein AM and 10  $\mu\text{M}$  propidium iodide in growth medium at 37  $^\circ\text{C}$  for 3 h. Cells were then washed twice with PBS, and cell images were acquired every 15 min with an inverted fluorescence microscope (Axiovert 40CFL, Carl Zeiss MicroImaging, Inc., Thornwood, NY), equipped with a mercury lamp and digital camera (ProgRes C3, JENOPTIK Laser, Jena, Germany). Images were captured using a Cy3 filter ( $\lambda_{\text{ex}}$  and  $\lambda_{\text{em}}$  of 535/50 and 590–700 nm, respectively) to detect propidium iodide-associated red fluorescence and a FITC filter ( $\lambda_{\text{ex}}$  and  $\lambda_{\text{em}}$  of 470/40 and 535/40 nm, respectively) to detect green fluorescence of

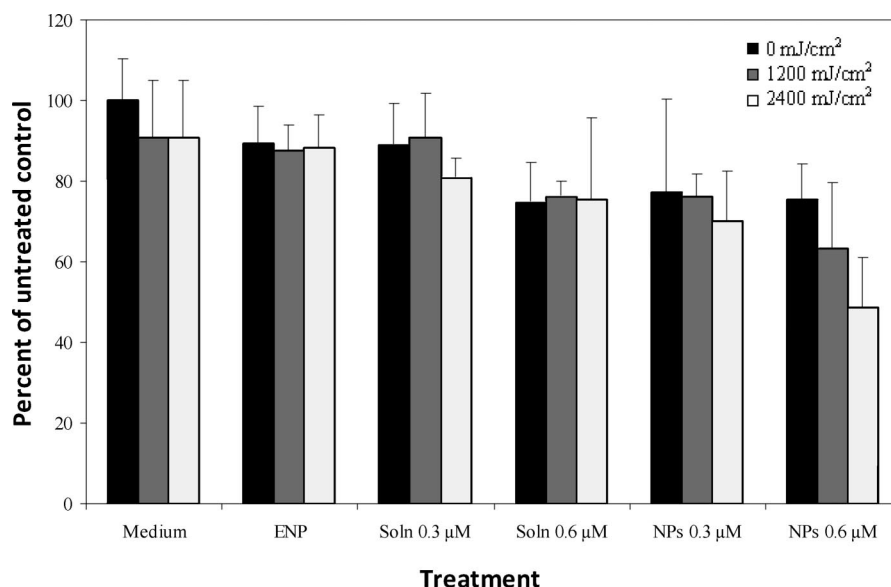


**Figure 5.** PDT with methylene blue in 4T1 cells. Cells were incubated for 24 h with growth medium (Medium), blank nanoparticles (ENP), methylene blue in solution (Soln), or methylene blue loaded nanoparticles (NPs). Cells were then exposed to different doses of light. Cell viability was quantified using MTS assay. Data as mean  $\pm$  SD ( $n = 8$  wells). \* $P < 0.05$ .

calcein. Cells that received just growth medium or an equivalent dose of empty nanoparticles along with light exposure were used as controls for methylene blue solution and methylene blue nanoparticles, respectively. Cells that received the same treatments without light exposure were used as dark controls.

**Intracellular Distribution of Methylene Blue.** MCF-7 cells were allowed to attach in 6-well plates (500,000 cell/well/mL) for 48 h. Cells were incubated with 2.7  $\mu$ M methylene blue in solution or encapsulated in nanoparticles for 2 h and then washed twice with PBS to remove any adherent nanoparticles. Cells were then trypsinized by incubation for 10 min with 0.5 mL of TrypLE (Invitrogen, Carlsbad, CA) at 37 °C and 5% CO<sub>2</sub>. Trypsinized cells were diluted in 1 mL of medium and transferred to 1.5 mL Eppendorf centrifuge tubes and centrifuged for 6 min at 100g. The cell pellet was collected and separated into cytosol and nuclear fractions using Nuclear/Cytosol fractionation kit according to the manufacturer’s instructions (BioVision, Mountain View, CA). Briefly, the cell pellet was suspended in 0.2 mL of cytosol extraction buffer-A mix (1 mL of cytosol extraction buffer-A mixed with 2  $\mu$ L of protease inhibitor cocktail and 1  $\mu$ L of dithiothreitol (DTT)) and vortexed vigorously to resuspend cells. After 10 min of ice-bath incubation, 11  $\mu$ L of ice-cold cytosol extraction buffer-B was added and then cells were vortexed. After 1 min of incubation on an ice-bath, cells were centrifuged for 5 min at 20000g. Immediately, the cytosolic fraction (supernatant) was transferred to prechilled centrifuge tubes and stored at  $-80$  °C until further use. The pellet was resuspended in 100  $\mu$ L of ice-cold nuclear extraction buffer mix (1 mL of nuclear extraction buffer mixed with 2  $\mu$ L of protease inhibitor cocktail and 1  $\mu$ L of DTT), vortexed vigorously and then incubated on an ice-bath for 10 min. Vortexing and incuba-

tion steps were repeated 4 times, and then cells were centrifuged for 10 min at 20000g. Immediately, the nuclear fraction (supernatant) was transferred to clean prechilled tubes and stored at  $-80$  °C for further analysis.

The protein content of the nuclear/cytosol fraction was determined using the Pierce BCA protein assay according to the manufacturer’s instructions (Pierce Biotechnology, Rockford, IL). Nuclear and cytosol fractions were extracted (Labquake shaker, Barnstead Thermolyne, Dubuque, IA) for 5 h in the dark at room temperature with 0.3 and 0.5 mL of methanol, respectively. The concentration of methylene blue in the methanolic extract was determined using HPLC (see Nanoparticle Characterization). The methylene blue concentration in the nuclear/cytosol extracts was normalized to the protein concentration of the corresponding fractionate.

**Microscopic Analysis of Intracellular Distribution of Methylene Blue.** MCF-7 cells were cultured on coverslips placed in 35 mm dishes (50,000 cells/dish) for 24 h. Cells were treated with 53  $\mu$ M methylene blue in solution or in nanoparticles. Two hours after addition of the treatments, cells were washed and incubated with 75 nM LysoTracker Green for 30 min. Cells were washed again and counterstained with 4’,6-diamidino-2-phenylindole (DAPI). Cell images were acquired using a BX60 Olympus fluorescence microscope. Images captured using the Cy3 filter were overlaid with those captured using FITC and DAPI filters to determine the localization of methylene blue in lysosomes and nucleus, respectively.

**Intracellular ROS Generation.** Intracellular ROS generation was investigated using CM-H<sub>2</sub>DCFDA. CM-H<sub>2</sub>DCFDA is acetylated carboxyl derivative of reduced fluorescein that is used as a cell-permeant indicator of ROS. CM-H<sub>2</sub>DCFDA is converted to fluorescein in the presence of ROS. MCF-7 cells were seeded in 6-well plates at 200,000 cell/well/3 mL

density. Following incubation with  $0.3 \mu\text{M}$  free or nanoparticle-encapsulated methylene blue for 24 h, cells were treated with  $10 \mu\text{M}$  CM-H<sub>2</sub>DCFDA. After 1 h incubation, cells were washed twice with PBS and then exposed to light ( $1200 \text{ mJ}/\text{cm}^2$ ). Immediately after light exposure and every 20 min after that, cell images were acquired using an inverted fluorescence microscope over a 3 h period. Images were captured in bright field and epi-fluorescence mode (FITC filter). Cells that received similar treatments without the light exposure were used as dark controls.

**ROS Generation *ex Vitro*.** To study the effect of encapsulation in nanoparticles on ROS production, methylene blue ( $0.3$  or  $0.6 \mu\text{M}$ ; free or encapsulated in nanoparticles) in PBS was exposed to light ( $1200 \text{ mJ}/\text{cm}^2$ ;  $665 \text{ nm}$ ) in the presence of  $10 \mu\text{M}$  3'-(*p*-aminophenyl) fluorescein (APF). APF is converted to fluorescein in the presence of ROS. APF has limited reactivity and high resistance to light-induced oxidation and is highly sensitive to hydroxyl radical ( $\cdot\text{OH}$ ), peroxyxynitrite anion ( $\cdot\text{ONOO}$ ) and hypochlorite anion ( $\cdot\text{OCl}$ ). Formation of fluorescein from APF was quantified by monitoring fluorescence at  $485/528 \text{ nm}$  using a fluorescence plate reader (FLX800, Bio-Tek Instruments, Winooski, VT). PBS and empty nanoparticles dispersed in PBS were used as controls. To study the effect of dose of light on ROS generation, samples were exposed to 10 consecutive doses of light ( $1200 \text{ mJ}/\text{cm}^2$  per dose) and the fluorescence generated was measured after each illumination. To determine the effect of inactive components of nanoparticles on ROS generation, free methylene blue was mixed with empty nanoparticles and treated as above. Above experiments repeated in the absence of light were used as light-negative controls.

Because the APF assay is not very sensitive for singlet oxygen species ( $^1\text{O}_2$ ), we also determined the effect of encapsulation in nanoparticles on the production of ( $^1\text{O}_2$ ). SOSGR is highly selective for ( $^1\text{O}_2$ ) with negligible response to  $\cdot\text{OH}$  or  $\cdot\text{O}_2$ . When SOSGR encounters ( $^1\text{O}_2$ ), it gets activated and forms a fluorescent product. Above experiments with APF were repeated in the presence of  $10 \mu\text{M}$  SOSGR. ( $^1\text{O}_2$ ) formed was quantified by measuring fluorescence at  $485/528 \text{ nm}$ .

**Statistical Analysis.** Student's *t* test was used to analyze the differences in cytotoxicities and in nuclear accumulation of methylene blue following treatment with free or nanoparticle-encapsulated methylene blue. Differences in ROS production among treatment groups were evaluated by ANOVA followed by planned comparison tests to evaluate pairwise comparisons among treatment groups. A probability level of  $p < 0.05$  was considered significant.

## Results

**Nanoparticle Characterization.** Nanoparticles were characterized for size, morphology, zeta potential and drug loading. Results of dynamic light scattering studies indicated that methylene blue-loaded nanoparticles had an average diameter of  $79 \text{ nm}$  with a polydispersity of  $0.052$ . AFM studies indicated that nanoparticles had a spherical morphol-

ogy, with an average diameter of  $72 \pm 11 \text{ nm}$  as determined by measuring the lateral width of particles using sectional analysis (Figure 1). Electrophoretic light scattering studies indicated that nanoparticles had a net negative surface charge of  $-19.3 \pm 1.3 \text{ mV}$ . Methylene blue was efficiently encapsulated in the nanoparticles ( $9.0 \pm 0.6\%$  w/w; encapsulation efficiency of  $82\%$ ).

**Tumor Cell Kill.** In order to determine the effect of encapsulation of methylene blue in nanoparticles, MCF-7 cells were exposed to light following treatment with free methylene blue or that encapsulated in nanoparticles. As can be seen from Figure 2A, encapsulation of methylene blue in nanoparticles enhanced the tumor cell kill over the dose range studied. Since the enhancement observed with nanoparticles was greater at lower doses, we selected two low doses ( $0.3$  and  $0.6 \mu\text{M}$ ) for further studies. At both of the doses, nanoparticle-encapsulated methylene blue demonstrated greater cytotoxicity than other treatment groups (Figure 2B,  $P < 0.05$  for both doses). Cells treated with empty nanoparticles showed insignificant cell killing, indicating the lack of photodynamic activity with blank nanoparticles in the dose range studied. Similarly, untreated cells that received light exposure alone showed no significant cell death. However, significant dark toxicity was observed with methylene blue treatment, especially at the  $0.6 \mu\text{M}$  dose ( $P < 0.05$  compared to untreated control).

We also evaluated whether the cytotoxicity observed following PDT was sustained over a period of time. As can be seen from Figures 3A and B, PDT resulted in a sustained inhibition of tumor cell growth over a period of 7 days, and nanoparticle treatment resulted in significantly better inhibition than free drug treatment at all times tested. It was interesting to note that methylene blue-induced dark toxicity was reversed to some extent at the end of 7 days, especially at the lower dose. MCF-7 cells used in this study have a doubling time of about  $36\text{--}48 \text{ h}$ . At the beginning of the experiment, the cells were seeded at about  $15\text{--}20\%$  confluence. Cells in the untreated group reached the plateau growth phase at the end of the study ( $90\text{--}100\%$  confluence). Treated cells were still in the logarithmic growth phase at the end of the study. Thus, cells in all of the groups were in the log phase over most of the study duration.

In order to determine the effect of dose of light on nanoparticle-mediated PDT, MCF-7 cells were treated with  $0.3 \mu\text{M}$  methylene blue and then exposed to different doses of light. As indicated by Figure 4, increasing the dose of the light resulted in a dose-dependent increase in cell kill for both free drug and nanoparticle treatments. Nanoparticle treatment resulted in a significantly higher cell kill at both of the light doses tested ( $P < 0.05$ ).

To study the effect of cell type on PDT-induced cytotoxicity, we determined the efficacy of nanoparticle-mediated PDT in 4T1 cells. 4T1 cells are highly metastatic tumor cells derived from murine mammary adenocarcinoma, and are, in general, more resistant to anticancer therapies than MCF-7 cells. 4T1 cells were more resistant than MCF-7 cells to PDT

with free methylene blue. Low methylene blue and light doses ( $0.3 \mu\text{M}$  and  $1200 \text{ mJ}/\text{cm}^2$ , respectively) did not affect the cell viability significantly (Figure 5). Similar to that observed in MCF-7 cells, encapsulation in nanoparticles significantly improved the cytotoxicity of methylene blue-mediated PDT. This trend was observed at all methylene blue and light doses.

We confirmed the enhanced PDT efficacy of nanoparticle-encapsulated methylene blue by determining the induction of necrosis following PDT in MCF-7 cells. Calcein stains live cells with green fluorescence while propidium iodide stains necrotic cells with red fluorescence. As can be seen from Figure 6, PDT with nanoparticle-encapsulated methylene blue resulted in a greater incidence of necrosis than that with other treatments.

**Subcellular Accumulation of Methylene Blue.** To determine the effect of encapsulation in nanoparticles on intracellular drug delivery, we compared the nuclear/cytosol accumulation of methylene blue following treatment with free and nanoparticle-encapsulated methylene blue. As Figure 7 indicates, treatment with methylene blue in nanoparticles resulted in significantly higher nuclear accumulation of the drug than that with free methylene blue ( $P < 0.05$ ). Total cellular accumulation of methylene blue was marginally higher following nanoparticle treatment than that following free drug treatment.

**Microscopic Analysis of Subcellular Distribution of Methylene Blue.** In order to study the effect of encapsulation in nanoparticles on the intracellular distribution of methylene blue, we determined the subcellular localization of the methylene blue-associated red fluorescence in MCF-7 cells following treatment with free and nanoparticle-encapsulated methylene blue. In this study, lysosomes were stained green using LysoTracker Green and nuclei were stained blue using DAPI. As can be seen from Figure 8, treatment with nanoparticles resulted in the accumulation of methylene blue inside nuclei and in lysosomal vesicles in the perinuclear region. Free methylene blue was found to accumulate mainly in the lysosomal vesicles, with very little nuclear distribution.

**Intracellular ROS Production.** In order to evaluate the effect of methylene blue encapsulation in nanoparticles on ROS production inside the cells, we compared ROS generation in MCF-7 cells following treatment with free and nanoparticle-encapsulated methylene blue. Treatment with nanoparticle-encapsulated methylene blue resulted in ROS production in significantly more number of cells than treatment with free drug (Figure 9). Light activation was necessary to achieve significant ROS production as demonstrated by very little green fluorescence in dark controls.

**Ex Vitro ROS and Singlet Oxygen Production.** To determine whether encapsulation in nanoparticles affected the ROS yield of methylene blue, we compared the ROS production after photoactivation of methylene blue in nanoparticles to that with free drug. In the assay used, ROS generation resulted in the conversion of APF to fluorescein, resulting in increased green fluorescence. Encapsulation of methylene blue in nanoparticles resulted

in significantly higher fluorescence (Figure 10,  $P < 0.05$ ), indicating increased ROS production with nanoparticle-encapsulated methylene blue. To evaluate the effect of dose of methylene blue on ROS yield, two different doses of methylene blue (equivalent to  $0.3$  or  $0.6 \mu\text{M}$ ) were used. At  $0.6 \mu\text{M}$  concentration, light-activation of methylene blue resulted in  $\sim 2$ -fold increase in fluorescence intensity compared to that at  $0.3 \mu\text{M}$  concentration. PBS and empty nanoparticles exposed to the same dose of light showed low levels of fluorescence, indicating negligible ROS production in the absence of methylene blue. We determined whether any of the nanoparticle components interacted with methylene blue to increase ROS production by exposing a simple physical mixture of empty nanoparticles and free methylene blue to light. Addition of blank nanoparticles to free methylene blue had no effect on ROS production by methylene blue (Figure 10).

We also evaluated the effect of encapsulation in nanoparticles on the production of singlet oxygen species [ $(^1\text{O}_2)$ ] by comparing  $(^1\text{O}_2)$  generation after light-activation of methylene blue in nanoparticles to that with free drug. Methylene blue encapsulated in nanoparticles resulted in significantly higher  $(^1\text{O}_2)$  production (Figure 11,  $P < 0.05$ ) compared to free methylene blue. The  $(^1\text{O}_2)$  generation increased linearly with increasing methylene blue concentration. In this experiment, we also evaluated the effect of nanoparticle components on  $(^1\text{O}_2)$  generation with methylene blue. Fluorescence generated with this simple mixture was higher than that with free methylene blue but was significantly less than that generated with nanoparticle-encapsulated methylene blue.

In order to determine whether methylene blue was utilized better when encapsulated in nanoparticles, we determined the ROS production when methylene blue was exposed to 10 consecutive doses of light ( $1200 \text{ mJ}/\text{cm}^2$  per dose). Fluorescence increased after each illumination, indicating increased production of ROS (Figure 12). Interestingly, the percent increase in ROS production actually increased slightly ( $P < 0.05$ ) at the end of the tenth dose for methylene blue in nanoparticles compared to that with free methylene blue. This suggests that nanoparticles did not necessarily alter the utilization of methylene blue for a given dose of light but rather increased the efficiency of ROS production from a given concentration of the photosensitizer.

## Discussion

Local generation of cytotoxic ROS, especially  $(^1\text{O}_2)$ , is considered the most important mechanism of cell kill following PDT.<sup>26,27</sup> Methylene blue, the photosensitizer used in this study, has been shown to generate  $(^1\text{O}_2)$  inside tumor cells upon activation with light of wavelength around  $665 \text{ nm}$ .<sup>19,28</sup> This ultimately results in organelle damage, single-strand DNA breaks, and cell death through induction of apoptosis and/or necrosis. However, clinical use of methylene blue in PDT has been limited due to the lack of significant efficacy after systemic administration.<sup>29</sup>

In this study, free methylene blue was moderately effective in inducing cytotoxicity in MCF-7 cells at the doses tested.

At higher doses ( $\geq 0.6 \mu\text{M}$ ) and longer time of incubation ( $\geq 24$  h), methylene blue caused significant dark toxicity. Dark toxicity with methylene blue and other photosensitizers has been previously reported.<sup>30,31</sup> It has been shown that, even in the absence of light exposure, methylene blue is more toxic to malignant cells than to normal cells.<sup>32</sup> Although the mechanism of methylene blue's dark toxicity has not been clearly established, dark toxicity was linked to the inhibition of soluble-guanylate cyclase and NADH oxidation.<sup>12,33</sup> It is possible that increased guanylate biosynthesis in cancer cells<sup>34</sup> could make the cancer cells more susceptible to methylene blue-induced dark toxicity. We found that the efficacy of PDT with methylene blue was cell line-dependent. MCF-7 cells were more susceptible than 4T1 cells to both light-induced and dark toxicities of methylene blue.

Encapsulation in nanoparticles significantly enhanced the cytotoxicity of methylene blue-mediated PDT. Cytotoxicity following PDT was responsive to both methylene blue and light doses, suggesting that the observed cytotoxicity was specifically due to the photodynamic effect of methylene blue. Studies with calcein and propidium iodide confirmed that nanoparticle-encapsulated methylene blue resulted in a higher incidence of necrosis than the free drug. The cytotoxicity observed following PDT was much more sustained for nanoparticle-treatment than for free drug treatment. It is possible that PDT following treatment with nanoparticle-encapsulated methylene blue resulted in significant cell damage, and therefore, the surviving cells took longer to recover. Also, we have previously shown that AOT-alginate nanoparticles sustain intracellular drug release,<sup>25</sup> which could have resulted in sustained dark toxicity in tumor cells. Further, it was interesting to note that nanoparticles significantly improved PDT efficacy in metastatic 4T1 cells. This is highly important, because metastasis continues to be highly untreatable and contributes to significant cancer-related mortality.<sup>35</sup>

Since intracellular generation of cytotoxic ROS is considered the most important mechanism of cell kill in PDT, we compared the intracellular ROS generation with free and nanoparticle-encapsulated methylene blue. Encapsulation in nanoparticles not only increased the ROS production within individual cells but also resulted in ROS production in a greater fraction of the cell population. This suggests that encapsulation in nanoparticles results in the delivery of photodynamic treatment to more tumor cells. It was also interesting to note that, while  $>90\%$  of the cells stained positive for ROS production (Figure 9), a smaller fraction of cells stained positive for necrosis (Figure 6) in the time period investigated (3 h). This suggests that PDT induces necrosis immediately in a fraction of treated cells and could probably induce other forms of cellular damage in other cells. Thus, it would be interesting to determine the differences in pathways of cell death following treatment with free and nanoparticle-encapsulated methylene blue.

We envisioned several potential reasons for the enhanced efficacy observed with nanoparticle-encapsulated methylene blue. First, nanoparticles could alter the subcellular distribution of encapsulated methylene blue. Previous studies have shown that the subcellular location of the photosensitizer is an important determinant of PDT efficacy.<sup>36</sup> Both quantitative and microscopic studies indicate that nanoparticles increased the nuclear accumulation of methylene blue while free drug treatment resulted in methylene blue accumulation in the cytosol and specifically in the lysosomal vesicles. Weak bases like methylene blue generally accumulate in the lysosomes following diffusion across the plasma membrane.<sup>37,38</sup> The cytoplasm has a physiologic pH while lysosomes are acidic. The acidic pH of lysosomes induces protonation of the weak base, limiting diffusion of ionized species across the lysosomal membrane into the cytoplasm (ion trapping). In addition, previous studies have shown that thiazine derivatives such as methylene blue also accumulate in the mitochondria.<sup>39,40</sup> Accumulation of methylene blue within mitochondria with high membrane potentials (such as those found in tumor cells) results in the conversion of methylene blue to the photochemically inactive leucomethylene blue and to partially active dimers, leading to a lowered yield of ( $^1\text{O}_2$ ) production within the cells.<sup>12</sup> The intracellular distribution of nanoparticles observed in the current study is in agreement with that observed in our previous study, where we reported that AOT-alginate nanoparticles entered the cell through endocytosis and resulted in the nuclear delivery of doxorubicin in drug-resistant tumor cells.<sup>41</sup> The mechanism of lysosomal escape and nuclear accumulation of AOT-alginate nanoparticles is not clear and needs further investigation.

(35) Sporn, M. B. The war on cancer: a review. *Ann. N.Y. Acad. Sci.* **1997**, *833*, 137–146.

(36) Walker, I.; Gorman, S. A.; Cox, R. D.; Vernon, D. I.; Griffiths, J.; Brown, S. B. A comparative analysis of phenothiazinium salts for the photosensitisation of murine fibrosarcoma (RIF-1) cells in vitro. *Photochem. Photobiol. Sci.* **2004**, *3*, 653–659.

(37) Diwu, Z.; Lown, J. W. Phototherapeutic potential of alternative photosensitizers to porphyrins. *Pharmacol. Ther.* **1994**, *63*, 1–35.

(38) Lin, C. W.; Shulok, J. R.; Kirley, S. D.; Cincotta, L.; Foley, J. W. Lysosomal localization and mechanism of uptake of Nile blue photosensitizers in tumor cells. *Cancer Res.* **1991**, *51*, 2710–2719.

(39) Ball, D. J.; Luo, Y.; Kessel, D.; Griffiths, J.; Brown, S. B.; Vernon, D. I. The induction of apoptosis by a positively charged methylene blue derivative. *J. Photochem. Photobiol. B* **1998**, *42*, 159–163.

(40) Oseroff, A. R.; Ohuoha, D.; Ara, G.; McAuliffe, D.; Foley, J.; Cincotta, L. Intramitochondrial dyes allow selective in vitro photolysis of carcinoma cells. *Proc. Natl. Acad. Sci. U.S.A.* **1986**, *83*, 9729–9733.

(41) Chavanpatil, M. D.; Khadair, A.; Gerard, B.; Bachmeier, C.; Miller, D. W.; Shekhar, M. P.; Panyam, J. Surfactant-polymer nanoparticles overcome P-glycoprotein-mediated drug efflux. *Mol. Pharmaceutics* **2007**, *4*, 730–738.

(42) Tijerina, M.; Kopeckova, P.; Kopecek, J. Mechanisms of cytotoxicity in human ovarian carcinoma cells exposed to free Mce6 or HPMA copolymer-Mce6 conjugates. *Photochem. Photobiol.* **2003**, *77*, 645–652.

(43) Tijerina, M.; Kopeckova, P.; Kopecek, J. Correlation of subcellular compartmentalization of HPMA copolymer-Mce6 conjugates with chemotherapeutic activity in human ovarian carcinoma cells. *Pharm. Res.* **2003**, *20*, 728–737.

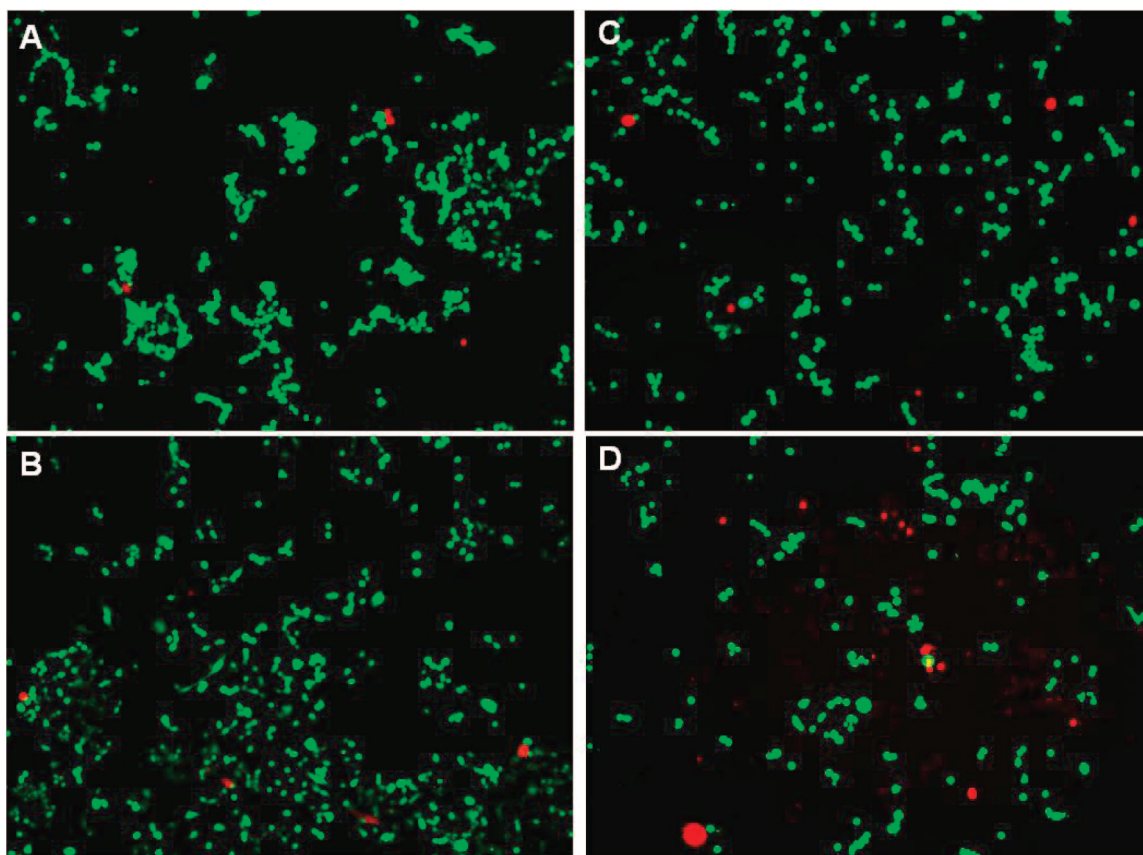


**Figure 6.** Induction of necrosis following PDT with methylene blue. MCF-7 cells were treated for 24 h with 0.3  $\mu\text{M}$  methylene blue in solution (A and B) or encapsulated in nanoparticles (C and D). Some of the groups (B and D) were exposed to light (1200  $\text{mJ}/\text{cm}^2$ , 665 nm) while others were used as dark controls (A and C). Cells were incubated with calcein-AM and PI and then imaged at 10 $\times$  using a fluorescence microscope under FITC (green) and Cy3 (red) filters. Images collected under the two filters were overlaid to determine necrotic (red) and viable (green) cells.

Increased nuclear localization could result in enhanced DNA damage following PDT, resulting in increased cytotoxicity observed with nanoparticle-encapsulated methylene blue. Similar increased cytotoxicity and necrosis has previously been observed for another photosensitizer, mesochlorin e6, when it was targeted to the nucleus.<sup>42,43</sup>

Enhanced efficacy of nanoparticle-encapsulated methylene blue can also be explained by the increased quantum yield of ROS production. Encapsulation in nanoparticles resulted in a significant increase in the formation of ( $^1\text{O}_2$ ) and other ROS. This was a surprising result, because previous studies have shown that encapsulation in a carrier generally reduces the ROS yield of methylene blue. For example, it was shown that encapsulation of methylene blue in magnetic silica nanoparticles resulted in a reduction in the ( $^1\text{O}_2$ ) yield.<sup>44</sup> Fabrication of magnetic silica particles required high alkaline pH, which could result in demethylation of methylene blue and the formation of its aggregates. This could have contributed to the reduction of ( $^1\text{O}_2$ ) yield compared to the free drug. Tang *et al.* have reported the encapsulation of methylene blue in 3 different nanocarriers; sol-gel, organically modified silica (ORMOSIL) and polyacrylamide matrices.<sup>19</sup> Among these 3 formulations, polyacrylamide matrix resulted in the highest ( $^1\text{O}_2$ ) yield, which, however, was

appreciably less than that obtained with the free drug. Reduction in ( $^1\text{O}_2$ ) yield was explained based on the effect of immobilization of the drug in the particle matrix and the effect of the particle's microenvironment.

It is not clear why encapsulation in AOT-alginate nanoparticles increased the ROS yield of methylene blue. Studies with other photosensitizers show that encapsulation in nanoparticles could either enhance or diminish the yield of ( $^1\text{O}_2$ ) and other ROS.<sup>19,45,46</sup> Sortino *et al.* has reported that nanoparticle-encapsulated porphyrin derivative retained the long-lived triplet state of the photosensitizer and resulted in a singlet oxygen quantum yield comparable to the free photosensitizer.<sup>45</sup> Gomes *et al.* reported enhanced singlet oxygen production with bacteriochlorophyll-a when encapsulated in poly(D,L-lactide-co-glycolide) nanoparticles.<sup>47</sup> In

(44) Tada, D. B.; Vono, L. L.; Duarte, E. L.; Itri, R.; Kiyohara, P. K.; Baptista, M. S.; Rossi, L. M. Methylene blue-containing silica-coated magnetic particles: a potential magnetic carrier for photodynamic therapy. *Langmuir* **2007**, *23*, 8194–8199.

(45) Sortino, S.; Mazzaglia, A.; Monsu Scolaro, L.; Marino Merlo, F.; Valveri, V.; Sciortino, M. T. Nanoparticles of cationic amphiphilic cyclodextrins entangling anionic porphyrins as carrier-sensitizer system in photodynamic cancer therapy. *Biomaterials* **2006**, *27*, 4256–4265.

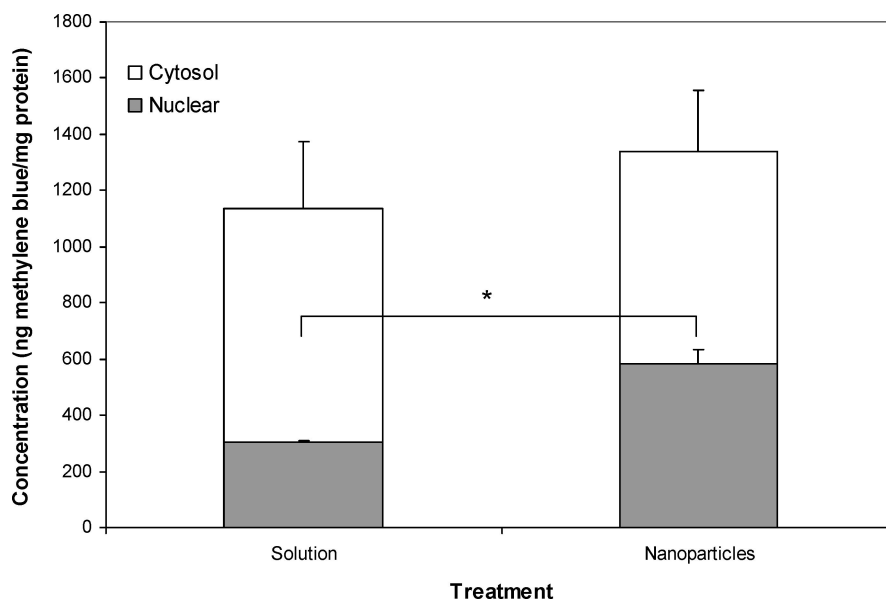


**Figure 7.** Nuclear accumulation of methylene blue. MCF-7 cells were incubated for 2 h with growth medium containing methylene blue in solution or encapsulated in nanoparticles. Cells were separated into nuclear and cytosolic fractions, and methylene blue concentration in nuclear/cytosol fractions was quantified using HPLC. Data as mean  $\pm$  SD ( $n = 3$ ). \* $P < 0.05$ ,  $t$  test.

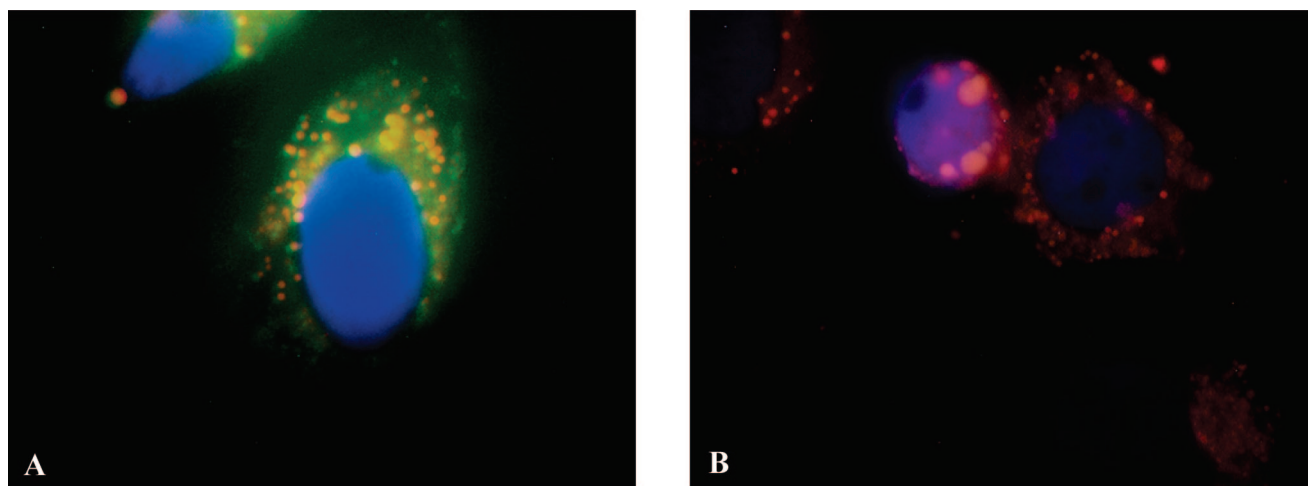


**Figure 8.** Intracellular distribution of methylene blue. MCF-7 cells were treated with methylene blue in solution (A) or in nanoparticles (B) for 2 h. Cells were rinsed, incubated with LysoTracker Green and then counterstained with DAPI. Cells were then imaged under FITC, Cy3 and DAPI filters using a 100 $\times$  objective. Images collected were overlaid to determine the colocalization of methylene blue (red) with lysosomes (green) and nucleus (blue).

the current study, it is possible that methylene blue was better utilized for ROS production when encapsulated in nanoparticles. If this was true, multiple exposures to light would result in successively lower ROS yields. Multiple illumina-

tion of encapsulated and free methylene blue showed increased ROS production after each illumination, with a significantly higher ROS yield in the nanoparticle group. In addition, at the end of the 10th dose of light, the difference in the cumulative ROS yield was significantly higher for the nanoparticle group than that for the free drug. This suggests that nanoparticles did not influence the utilization of methylene blue. Vakrat-Haglili *et al.* reported that the microenvironment surrounding the photosensitizer during light activation significantly affects the ROS yield both *in vitro* and *in vivo*.<sup>48</sup> This includes molecular oxygen<sup>49</sup> and other surrounding compounds,<sup>7</sup> pH<sup>50</sup> and hydrophobicity of the milieu.<sup>51,52</sup> Activated photosensitizer can abstract hydrogen

- (46) Roy, I.; Ohulchanskyy, T. Y.; Pudavar, H. E.; Bergey, E. J.; Oseroff, A. R.; Morgan, J.; Dougherty, T. J.; Prasad, P. N. Ceramic-based nanoparticles entrapping water-insoluble photosensitizing anticancer drugs: a novel drug-carrier system for photodynamic therapy. *J. Am. Chem. Soc.* **2003**, *125*, 7860–7865.
- (47) Gomes, A. J.; Lunardi, L. O.; Marchetti, J. M.; Lunardi, C. N.; Tedesco, A. C. Photobiological and ultrastructural studies of nanoparticles of poly(lactic-co-glycolic acid)-containing bacteriochlorophyll-a as a photosensitizer useful for PDT treatment. *Drug Delivery* **2005**, *12*, 159–164.

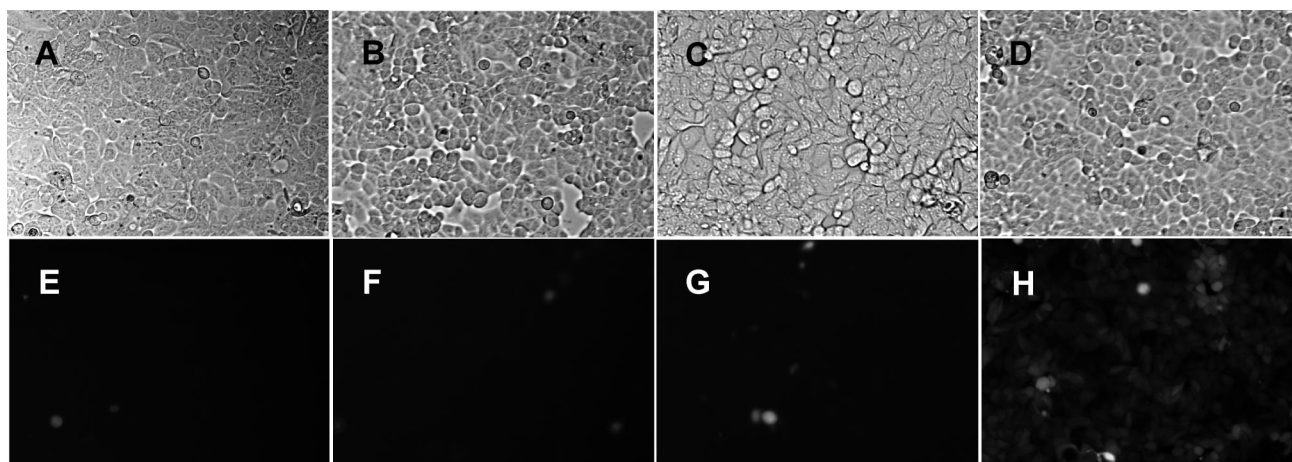


**Figure 9.** Intracellular ROS production following PDT with methylene blue. MCF-7 cells were treated for 24 h with methylene blue in solution (A, C, E, G) or encapsulated in nanoparticles (B, D, F, H). Cells were incubated with 10  $\mu$ M CM-H<sub>2</sub>DCFDA for 1 h, and some groups (C, D, G, H) were exposed to light (1200 mJ/cm<sup>2</sup>, 665 nm) while others (A, B, E, F) were used as dark controls. Cells were then visualized under bright field (top panel) or under epi-fluorescence (bottom panel) using a 10 $\times$  objective.

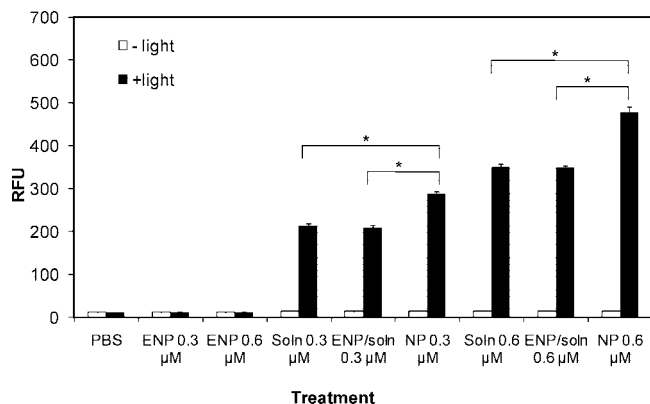


**Figure 10.** *Ex vitro* ROS production with methylene blue. Methylene blue in solution (Soln), encapsulated in nanoparticles (NP) or in physical mixture with empty nanoparticles (ENP/Soln) was dispersed in PBS and then exposed to light (1200 mJ/cm<sup>2</sup>) at 665 nm wavelength in the presence of APF. Fluorescence was measured using a fluorescence plate reader. Data as means  $\pm$  SD ( $n = 6$ ). \* $P < 0.05$ .

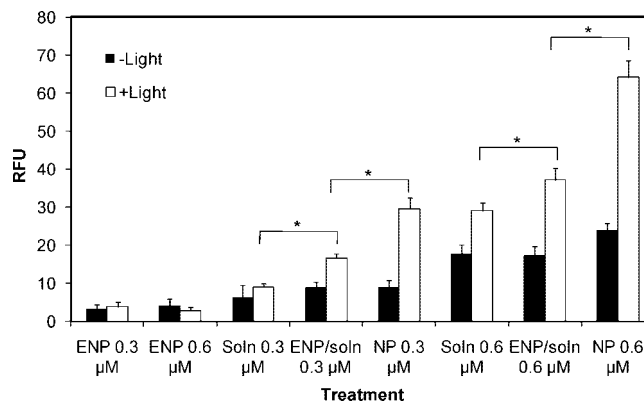


**Figure 11.** *Ex vitro* singlet oxygen species (<sup>1</sup>O<sub>2</sub>) production with methylene blue. Methylene blue in solution (Soln), encapsulated in nanoparticles (NP) or in physical mixture with empty nanoparticles (ENP/Soln) was dispersed in PBS and then exposed to light (1200 mJ/cm<sup>2</sup>) at 665 nm wavelength in the presence of SOSGR. Fluorescence was measured using a fluorescence plate reader. Data as means  $\pm$  SD ( $n = 6$ ). \* $P < 0.05$ .

atom(s) from surrounding molecules, generating free radicals. Electrons are then transferred to molecular oxygen, resulting in production of (<sup>1</sup>O<sub>2</sub>). It is possible that AOT–alginate nanoparticles provide a suitable environment for ROS production. Nanoparticles used in this work are expected to have an inner core of calcium-cross-linked alginate and AOT head groups, surrounded by one or more layers composed of AOT tails.<sup>22,25</sup> While a significant fraction of methylene blue is expected to be encapsulated in the core, some of the drug may exist on the surface of the particles. AOT has a sulfosuccinate group and alginate molecules possess carboxyl groups, both of which are considered good electron acceptors and hydrogen donors to facilitate a free radical reaction. Our *ex vitro* studies with a physical mixture of empty nanoparticles and methylene blue did not demonstrate an increase

in the general ROS production but did show an increase in the (<sup>1</sup>O<sub>2</sub>) formation. This indicates that nanoparticle components could contribute to the production of (<sup>1</sup>O<sub>2</sub>). However, it is clear that for maximal ROS production, methylene blue has to be in close proximity with the nanoparticle components, i.e., encapsulated inside nanoparticles.

Although not investigated in the study, another possible explanation for the enhanced efficacy of nanoparticles is that nanoparticle-encapsulated methylene blue is protected from cellular and extracellular reduction. While there are no cellular components in the *ex vitro* study to explain enhanced ROS production with nanoparticles, protection from degradation could, at least in part, contribute to the improved cytotoxicity observed in the cell culture studies. Previous studies with other formulations have demonstrated that

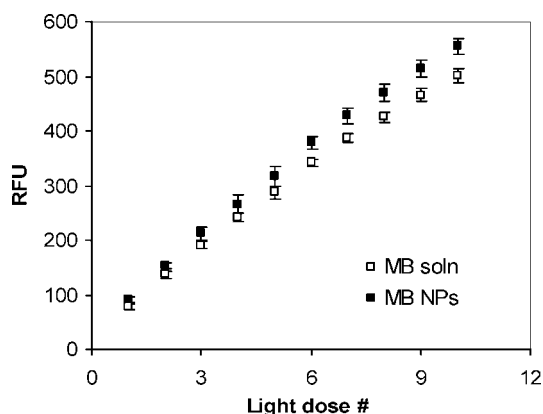


**Figure 12.** Effect of multiple doses of light on *ex vitro* ROS production with methylene blue. Methylene blue in solution (MB soln) or encapsulated in nanoparticles (MB NPs) was dispersed in PBS and then exposed to 10 consecutive doses (1200 mJ/cm<sup>2</sup> per dose) of light at 665 nm wavelength in the presence of APF. Fluorescence generated was measured using a plate reader. Data as means  $\pm$  SD ( $n = 8$ ). \* $P < 0.05$ .

nanoparticles could protect the encapsulated drug from degrading environments.<sup>53–55</sup>

- (48) Vakrat-Haglili, Y.; Weiner, L.; Brumfeld, V.; Brandis, A.; Salomon, Y.; McLlroy, B.; Wilson, B. C.; Pawlak, A.; Rozanowska, M.; Sarna, T.; Scherz, A. The microenvironment effect on the generation of reactive oxygen species by Pd-bacteriopheophorbide. *J. Am. Chem. Soc.* **2005**, *127*, 6487–6497.
- (49) Alvarez, M. G.; Prucca, C.; Milanesio, M. E.; Durantini, E. N.; Rivarola, V. Photodynamic activity of a new sensitizer derived from porphyrin-C60 dyad and its biological consequences in a human carcinoma cell line. *Int. J. Biochem. Cell Biol.* **2006**, *38*, 2092–2101.

## Conclusions

Encapsulation of methylene blue in AOT–alginate nanoparticles enhanced its photodynamic efficacy *in vitro*. Enhanced nuclear accumulation and increased ROS production contribute to the enhanced PDT efficacy of nanoparticle-encapsulated methylene blue. Based on these results, we conclude that the AOT–alginate nanoparticle system is a promising delivery vehicle for anticancer PDT with methylene blue.

**Acknowledgment.** Funding support from Wayne State University’s Research Enhancement Program is gratefully acknowledged.

MP800026T

- (50) Bronshtein, I.; Smith, K. M.; Ehrenberg, B. The effect of pH on the topography of porphyrins in lipid membranes. *Photochem. Photobiol.* **2005**, *81*, 446–451.
- (51) Cao, Y.; Koo, Y. E.; Koo, S. M.; Kopelman, R. Ratiometric singlet oxygen nano-optodes and their use for monitoring photodynamic therapy nanoplatforms. *Photochem. Photobiol.* **2005**, *81*, 1489–1498.
- (52) Rotta, J. C.; Lunardi, C. N.; Tedesco, A. C. Nitric oxide release from the S-nitrosothiol zinc phthalocyanine complex by flash photolysis. *Braz. J. Med. Biol. Res.* **2003**, *36*, 587–594.
- (53) Tang, W.; Xu, H.; Park, E. J.; Philbert, M. A.; Kopelman, R. Encapsulation of methylene blue in polyacrylamide nanoparticle platforms protects its photodynamic effectiveness. *Biochem. Biophys. Res. Commun.* **2008**, *369*, 579–583.
- (54) Dange, C.; Vranckx, H.; Balschmidt, P.; Couvreur, P. Poly(alkyl cyanoacrylate) nanospheres for oral administration of insulin. *J. Pharm. Sci.* **1997**, *86*, 1403–1409.
- (55) He, X. X.; Wang, K.; Tan, W.; Liu, B.; Lin, X.; He, C.; Li, D.; Huang, S.; Li, J. Bioconjugated nanoparticles for DNA protection from cleavage. *J. Am. Chem. Soc.* **2003**, *125*, 7168–7169.